Amphiphilic Polymers for Aggregation-Induced Emission at Air/Liquid Interfaces

Pablo G. Argudo,[1,‡] Nian Zhang,[2,3,‡] Hui Chen,[3] Gustavo de Miguel,[1] María T. Martín-Romero,[1] Luis Camacho,[1] Min-Hui Li,[2,3,] Juan J. Giner-Casares[1,*]*

[1]Departamento de Química Física y T. Aplicada, Instituto Universitario de Nanoquímica IUNAN, Facultad de Ciencias, Universidad de Córdoba (UCO), Campus de Rabanales, Ed. Marie Curie, E-14071 Córdoba, Spain

[2]Beijing Advanced Innovation Center for Soft Matter Science and Engineering, Beijing University of Chemical Technology, 100029 Beijing, China.

[3]Chimie ParisTech, PSL University Paris, CNRS, Institut de Recherche de Chimie Paris-UMR8247, 11 Rue Pierre et Marie Curie, 75231 Paris Cedex 05, Paris, France

ABSTRACT

Polymersomes and related self-assembled nanostructures displaying Aggregation-Induced Emission (AIE) are highly relevant for plenty of applications in imaging, biology and functional devices. Experimentally simple, scalable and universal strategies for on-demand self-assembly of polymers rendering well-defined nanostructures are highly desirable. A purposefully designed combination of amphiphilic block copolymers including tunable lengths of hydrophilic polyethylene glycol (PEG_m) and hydrophobic AIE polymer poly(tetraphenylethylene-trimethylenecarbonate) ($P(TPE\text{-}TMC)_n$) has been studied at the air/liquid interface. The unique 2D assembly properties have been analyzed by thermodynamic measurements, UV-vis reflection spectroscopy and photoluminescence in combination with molecular dynamics simulations. The $(PEG)_m$-*b*-$P(TPE\text{-}TMC)_n$ monolayers formed tunable 2D nanostructures self-assembled on demand by adjusting the available surface area. Tuning of the PEG length allows to modification of the area per polymer molecule at the air/liquid interface. Molecular detail on the arrangement of the polymer molecules and relevant molecular interactions has been convincingly described. AIE fluorescence at the air/liquid interface has been successfully achieved by the $(PEG)_m$-*b*-$P(TPE\text{-}TMC)_n$ nanostructures. An experimentally simple 2D to 3D transition allowed to obtain 3D polymersomes in solution. This work suggests that engineered amphiphilic polymers for AIE may be suitable for selective 2D and 3D self-assembly for imaging and technological applications.

INTRODUCTION

Aggregation-induced emission (AIE) is being revealed as a core functionality in self-assembled nanostructures with highly promising applications in plenty of areas.[1,2] AIE is promoted by the aggregation of chromophore groups. The AIE chromophores that show no fluorescence in molecularly soluble state can display significant fluorescence when forming aggregates. The detailed photophysical mechanism for AIE is still under debate, with certain AIE related with the restricted intramolecular rotation of the chromophore groups in the aggregates.[3] A “dark state” concerning excited states has also been proposed to account for the appearance of AIE.[4] The AIE properties can be obtained by subtle chemical modifications of the chromophore groups.[5,6]

AIE is used in a wide range of applications, with biomedicine as the forefront field. Biomedical sensing might greatly benefit from the AIE.[7] In situ monitoring of cellular processes as apoptosis during in vivo experiments was successfully carried out using AIE.[8] Imaging of tumor cells in hypoxia regime has been demonstrated using AIE.[9] Emission in the NIR range from AIE fluorophores were developed for cancer imaging.[10] In addition to sensing, AIE can be combined with programmed delivery using purposefully designed nanoparticles.[11] Photodynamic therapy (PDT) has also been demonstrated using AIE-based nanoparticles.[12] Both PDT and sensing functionalities could be simultaneously incorporated in AIE luminogens for selective detection and killing of Gram-positive bacteria.[13,14] Thus, AIE-based molecules are proposed as a relevant strategy for effective biocides against resistant bacteria.[15] Nanocarriers for pancreatic cancer therapy using AIE groups have also been proposed.[16]

Beyond biomedical applications, the use of AIE-based nanostructures has been demonstrated in mechanical sensing[17] and responsive self-assembly under exposure to carbon dioxide.[18] AIE derivatives can be used in forensics for revealing fingerprints.[19] Sensing of explosives using

AIE has also been demonstrated.[20] Although AIE can be displayed by small chemical group, AIE-polymers incorporate a high versatility for self-assembly given the possibility of varying chemical composition and polymer length. In this sense, amphiphilic block copolymers allocate for self-assembly and fluorescence in intracellular imaging.[21] Different blocks have been tested in AIE-copolymers, e.g., polyurethane for selective imaging of actin in living cells.[22]

Block copolymers $(PEG)_m$-*b*-$P(TPE\text{-}TMC)_n$ combining polyethylene glycol $(PEG)_m$ and polytrimethylene carbonate $P(TPE\text{-}TMC)_n$ have been proven to efficiently self-assemble in bulk solution to polymersomes displaying AIE in our previous work.[23] The PEG block provides adequate hydrophilicity to achieve amphiphilic block copolymer, while simultaneously being biocompatible and repellent for adsorption of proteins.[24] Therefore, the PEG block is a relevant choice for the hydrophilic block of the amphiphilic copolymer in terms of physicochemical features and relevance in biological applications. The tetraphenylethylene chromophore is highly relevant in AIE as a forefront building block. The possible use of tetraphenylethylene in pharmacological formulations is still a matter of research and clinical essays.[25,26] On the other hand, published reports clearly show the applicability of the tetraphenylethylene chromophore group in imaging and photodynamic therapy in model cell studies.[27,28] Therefore, the AIE block was based on tetraphenylethylene for our AIE amphiphilic polymers. Herein, a series of PEG_m-*b*-$P(TPE\text{-}TMC)_n$ derivatives with larger choices of lengths of both polymer blocks have been designed, and their directed 2D self-assembly on air/liquid interface has been investigated in detail. The intermolecular interactions were tuned by adjusting the length of each block. The PEG length has been increased to about three-fold and the $P(TPE\text{-}TMC)_n$ length to about two-fold with respect to our previous study.[23] The surface area per $(PEG)_m$-*b*-$(TPE\text{-}TMC)_n$ molecule was finely adjusted by the Langmuir technique. Detailed information on the molecular arrangement at the

air/liquid interface was obtained by devoted experimental techniques, mainly UV-vis reflection spectroscopy[29] and photoluminescence spectroscopy. The adjustment of the available surface area has been proven a successful strategy for tuning the mechanical stimulus of surface pressure in 2D, allowing the directed self-assembly of nanoparticles at the air/liquid interface.[30] In addition to studying the molecular arrangement, hierarchical materials can be build using this approach at the air/liquid interface guided by polymers.[31] Remarkably, application of bulk pressure in 3D crystals of anthracene-TPE derivatives has also been reported as an efficient physical stimulus for promoting AIE.[32] The standard 3D stimuli for obtaining AIE, e.g., variation of concentration and solvent composition are translated into the 2D using the simple mechanical stimulus. Quantitative insights on the physical scenario and the chemical design of block copolymers for obtaining AIE have also been explored in this study. This study aims at the understanding of the physicochemical behavior of model AIE amphiphilic polymers for all applications including self-assembly of the AIE polymers.

RESULTS AND DISCUSSION

The general molecular structure of the $(PEG)_m$-*b*-P$(TPE\text{-}TMC)_n$ derivatives is shown in Figure 1A. The tuning of the intermolecular interactions was achieved by adjusting the length of the hydrophilic and hydrophobic blocks. The functionality of each block in the self-assembly process is clearly defined. The PEG block contributed to hydrophilic interactions with water, greatly stabilizing the $(PEG)_m$-*b*-P$(TPE\text{-}TMC)_n$ monolayer at the air/liquid interface. The P$(TPE\text{-}TMC)_n$ block directed the self-assembly by hydrophobic interaction to achieve aggregation-induced emission (AIE) at the air/liquid interface (see Figure 1B). Ten derivatives of $(PEG)_m$-*b*-P$(TPE\text{-}TMC)_n$ with different m and n values have been used in this study (see Table 1).

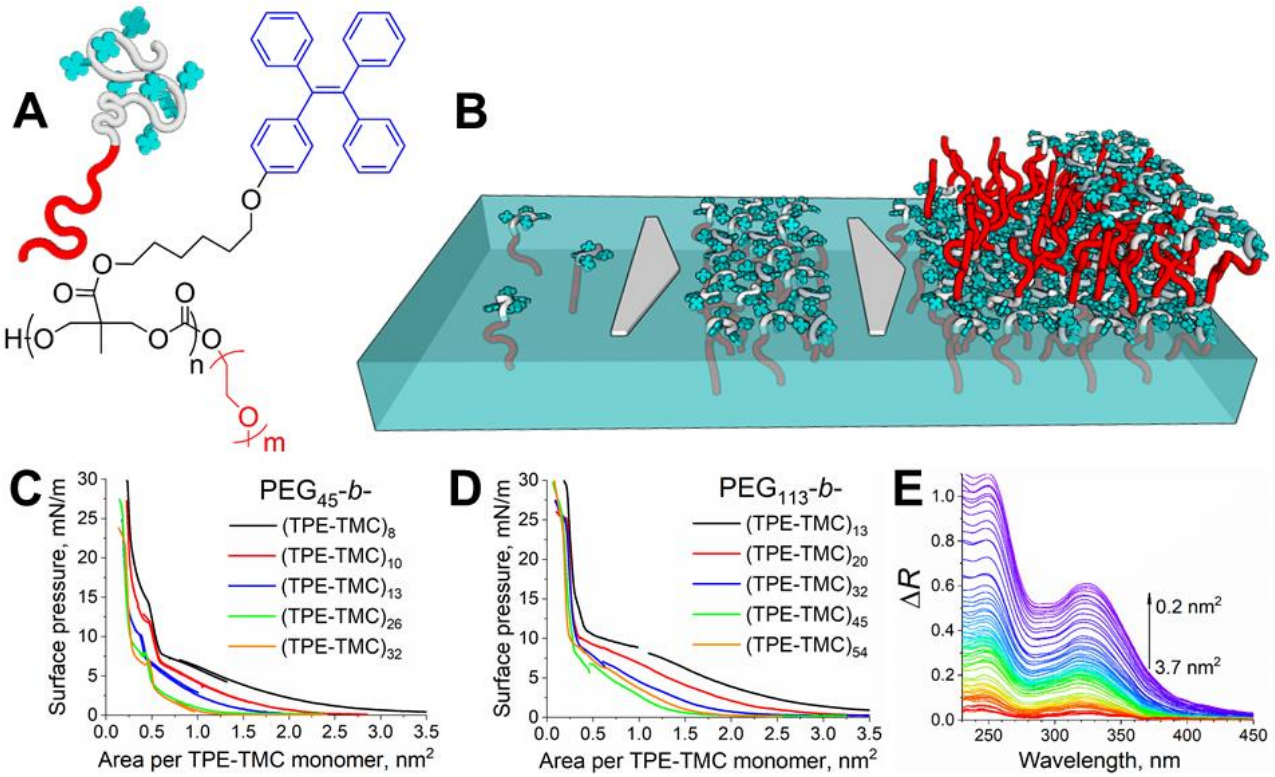

Figure 1. 2D self-assembly and in situ UV-vis reflection spectroscopy of AIE polymers. A) Molecular structure of the PEG_m-*b*-P(TPE-TMC)$_n$ polymer. B) Sketch depicting the self-assembly of the PEG_m-*b*-P(TPE-TMC)$_n$ polymer at the air/water interface C) Surface pressure – molecular area isotherms for the PEG_{45} polymer derivatives. D) Surface pressure – molecular area isotherms for the PEG_{113} polymer derivatives. E) UV-vis reflection spectra of the PEG_{45}-*b*-P(TPE-TMC)$_8$ monolayer recorded from 3.7 to 0.2 nm^2 per TPE monomer.

Table 1. Chemical composition of the $(PEG)_m$-*b*-P(TPE-TMC)$_n$ derivatives.

PEG_{45}-*b*-P(TPE-TMC)$_n$			
Polymer name	Mn[a]	PDI[b]	f_{PEG} (%)[a]
PEG_{45}-*b*-P(TPE-TMC)$_8$	6800	1.34	29
PEG_{45}-*b*-P(TPE-TMC)$_{10}$	8100	-	25
PEG_{45}-*b*-P(TPE-TMC)$_{13}$	9600	1.35	21

PEG_{45}-*b*-P(TPE-TMC)$_{26}$	17100	-	12
PEG_{45}-*b*-P(TPE-TMC)$_{32}$	20900	1.44	9.6
PEG_{113}-*b*-P(TPE-TMC)$_n$			
Polymer name	Mn[a]	PDI[b]	f_{PEG} (%)[a]
PEG_{113}-*b*-P(TPE-TMC)$_{13}$	12700	1.47	39
PEG_{113}-*b*-P(TPE-TMC)$_{20}$	17100	1.36	29
PEG_{113}-*b*-P(TPE-TMC)$_{32}$	23900	1.37	21
PEG_{113}-*b*-P(TPE-TMC)$_{45}$	31400	1.47	16
PEG_{113}-*b*-P(TPE-TMC)$_{54}$	37000	1.44	13.5

[a]The number-average molecular weight (M_n) and the hydrophilic weight ratio (over the total copolymer) (f_{PEG}) of the copolymer were determined by ^{1}H NMR spectroscopy.

[b]PDI = Mw/Mn; Mw and Mn here were measured by size exclusion chromatography using THF as eluent and monodispersed polystyrenes as calibration standards.

The available surface area per molecule of PEG_m-*b*-P(TPE-TMC)$_n$ monomer and polymer molecule at the air/liquid interface could be conveniently controlled, see surface pressure-molecular area isotherms Figure 1 and S1, respectively. Given the large values of area per polymer molecule, the surface pressure-molecular area isotherms could not be recorded in a single run due to lack of available area of the Langmuir trough. Therefore, the isotherms were recorded at different values of starting molecular area. Remarkably, the isotherms were highly reproducible, with an almost complete overlap between the sections of the isotherms.

A 2D fluid phase was expected for high values of available surface area in agreement with amphiphilic PEG-derivatives of phospholipids.[33] No liquid expanded - liquid condensed phase transition was shown in the isotherms, as expected from the exotic design of the amphiphilic polymers in contrast to standard surfactants.[34,35] The increase of the length of the P(TPE-TMC)

block led to an increase of monolayer condensation and the shift of the curve towards smaller values of areas per monomer. An enhancement of the packing of the PEG_m-*b*-P(TPE-TMC)$_n$ molecules was obtained with the increase of the length of the P(TPE-TMC) block, indicating a more condensed assembly of the polymer molecules at the air/liquid interface. In other words, increasing the length of the P(TME-TMC) block led to a decrease in the area per PEG_m-*b*-P(TPE-TMC)$_n$ molecule in a given monolayer at the air/liquid interface. Self-assembled 2D structures from AIE amphiphilic block copolymers with higher length of the hydrophobic AIE block are expected from the data at the air/liquid interface to contain a higher number of molecules per particle of similar size, e. g., micelles, vesicles, nanotubes.[36–39] Therefore, the adjustment of the length of the P(TPE-TMC) block might be used as a tool for tuning the interplay between the number of AIE polymer molecules and size of the self-assembled nanostructure.

The self-organization of the PEG_{113}-*b*-P(TPE-TMC)$_n$ was different to the PEG_{45}-*b*-P(TPE-TMC)$_n$ polymer molecules at the air/water interface, leading to a different course of the surface pressure-molecular area isotherms. A single kink was observed at ca. 0.4 nm^2 per polymer for PEG_{113} series, whereas two kinks were obtained for the PEG_{45} series. PEG_m-*b*-P(TPE-TMC)$_n$ monolayers subjected to a further reduction of the surface area led to polymer molecules tightly packed at the air/liquid interface. This state has been traditionally related with a highly stretched configuration of the PEG chains named as “brush regime” of the PEG chains.[40] However, the “brush regime” has been questioned by Salesse et al., who proposed instead the presence of collapsed structures under high values of surface pressure that stayed attached to the monolayer.[41] Detailed computational simulations on the arrangement of the PEG block support this scenario, see below. Moreover, the area per P(TPE-TMC) block for highly compressed PEG_m-*b*-P(TPE-TMC)$_n$ monolayers was ca. 0.2 nm^2, significantly lower than the expected area of ca.

0.45 nm^2 per P(TPE-TMC) block. This discrepancy in the values of surface area per P(TPE-TMC) block might be ascribed to the formation of multilayer supramolecular structures or to a loss of polymer molecules into the bulk water subphase. Therefore, the difference in the transition points, i.e., kinks, for the isotherms of PEG_{113} and PEG_{45} series arise from different degree of formation of multilayers as shown below by UV-vis reflection spectroscopy. Note that in all cases a homogeneous structure at the interface was observed by in situ Brewster Angle Microscopy, see Figures S2-11. The excellent self-assembly properties of the amphiphilic polymers were verified by the absence of any micrometric domains or phase segregation.

The surface concentration and state of aggregation of PEG_m-*b*-P(TPE-TMC)$_n$ monolayers could be monitored in situ at the air/liquid interface by following the signal of the P(TPE-TMC) block at the interface using UV-vis reflection spectroscopy.[42] See Fig. 1E for a representative example including UV-vis reflection spectra of the PEG_{45}-*b*-P(TPE-TMC)$_8$. The UV-vis reflection signal neglects any contribution from the bulk solution, instead arising exclusively from the enhancement of reflection of the incoming radiation by absorbance of molecules located at the air/liquid interface according to the equation (1):

$$\Delta R \simeq 2.303 \cdot 10^3 \, f_0 \varepsilon \sqrt{R_S} \Gamma \qquad (1)$$

where ΔR is the increase of reflection under normal incidence, ε is the molar absorption coefficient ($M^{-1} \cdot cm^{-1}$), R_S is the reflectivity of the aqueous interface (0.0196), Γ is the surface concentration of the P(TPE-TMC) block ($mol \cdot cm^{-2}$), and f_0 is the orientation factor. Using the value of $\varepsilon = 2.04 \cdot 10^4$ $M^{-1} \cdot cm^{-1}$ from our previous study on similar polymers[23] and A as the available surface area for the P(TPE-TMC) block, the orientation factor can be related with the recorded intensity of the UV-vis reflection signal using equation (2):

$$\Delta R_n = \Delta R \cdot A = 0.11 \cdot f_0 \qquad (2)$$

The UV-vis reflection spectra for the PEG_{45}-*b*-P(TPE-TMC)$_8$ and PEG_{113}-*b*-P(TPE-TMC)$_{20}$ monolayers are shown in Figure 2. A significant signal was present at highly expanded state of the monolayer, indicating the presence of the TPE groups at the air/liquid interface. The subtraction of UV-vis reflection spectra normalized to the available area per P(TPE-TMC) block ($\Delta R_n = \Delta R \cdot A$) with respect to the normalized UV-vis reflection spectrum at 2 nm^2 per P(TPE-TMC) block ($\Delta R_{n,0}$) is expressed as [ΔR_n - $\Delta R_{n,0}$]. The $\Delta R_{n,0}$ value was taken as a reference value for a PEG_m-*b*-P(TPE-TMC)$_n$ with single monolayer structure. Thus a value of [ΔR_n - $\Delta R_{n,0}$] greater than zero indicates the presence of multilayer. The value of [ΔR_n - $\Delta R_{n,0}$] informs on both the formation of multilayered structure of the PEG_{113}-*b*-P(TPE-TMC)$_{20}$ polymer molecules and aggregation of the P(TPE-TMC) block at the air/liquid interface, see Figure 2. The PEG_{45}-*b*-(TPE-TMC)$_8$ monolayer showed formation of multilayered structure from 0.44 nm^2 to lower values of area per P(TPE-TMC) block as evidenced by the positive value of [ΔR_n - $\Delta R_{n,0}$], see Figure 2. A reduction of the available surface area led to an increase of the [ΔR_n - $\Delta R_{n,0}$] spectra, indicating the propagation of the multilayer structure over the monolayer. Therefore, the [ΔR_n - $\Delta R_{n,0}$] spectra greater than zero for all polymers upon compression of the monolayer indicates the ability to form multilayered structures at the air/water interface. The detailed organization within the multilayers is discussed below.

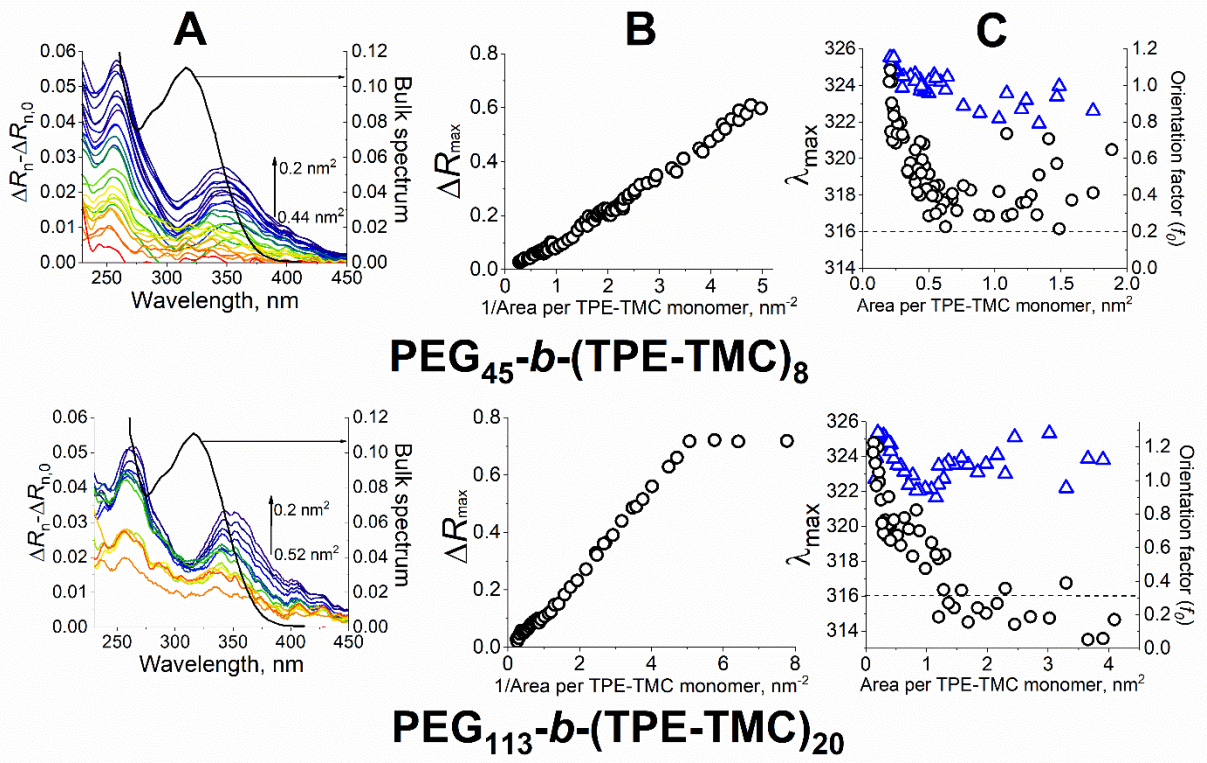

Figure 2. In situ UV-vis reflection spectroscopy for the AIE-polymers at the air/liquid interface. Top: PEG_{45}-*b*-$(TPE\text{-}TMC)_8$ monolayer. Bottom: PEG_{113}-*b*-$(TPE\text{-}TMC)_{20}$ monolayer. A) Left: difference normalized UV-vis reflection spectra. Right: Bulk UV-vis spectrum (black line). Inset: values of area per P(TPE-TMC) block. B) Maximum value of intensity of UV-vis reflection. C) Left, position of the UV-vis reflection peak (black circles). Dashed line corresponds to the peak position for the UV-vis absorbance spectrum in bulk solution. Right, orientation factor for the TPE groups (blue triangles).

The UV-vis reflection signal increased with compression of the monolayer up to the maximum value of UV-vis signal for a surface concentration of 0.2 nm^2 per P(TPE-TMC) block. The value of maximum intensity of the UV-vis reflection signal (ΔR_{max}) was inversely proportional to the available surface area per P(TPE-TMC) block, see Figure 2B. The UV-vis reflection intensity followed a linear trend for the PEG_{45}-*b*-$(TPE\text{-}TMC)_8$ monolayer, indicating no loss of copolymer

into the bulk water. A similar value of ΔR_{max} for the PEG_{113}-*b*-$(TPE\text{-}TMC)_{20}$ monolayer was achieved at low values of surface area. However, in this case a limiting value of ΔR_{max} of ca. 0.75 was obtained for 5 nm^{-2}, which corresponds to 0.2 nm^2 per P(TPE-TMC) block.

Considering a value of the orientation factor of $f_0 = 1$ corresponding to a random distribution and a minimum value of area of 0.45 nm^2 per P(TPE-TMC) block, a highly packed monolayer of $(PEG)_m$-*b*-$P(TPE\text{-}TMC)_n$ at the air/liquid interface should display a maximum value of $\Delta R = 0.24$. Higher values of ΔR could be achieved exclusively by the formation of multilayer supramolecular structures at the air/liquid interface. A value of $\Delta R_{max} = 0.6$ was found for the PEG_{45}-*b*-$(TPE\text{-}TMC)_8$ monolayer at 5 nm^{-2}, i.e., 0.2 nm^2 per TPE group. Similar values were found for the PEG_{45}-*b*-$(TPE\text{-}TMC)_n$ polymer series, indicating that the PEG_{45} block led in all cases to an incomplete trilayer structure. The intensity of the UV-vis reflection signal ΔR_{max} indicated a multilayered structure, including both bilayer and trilayer regions. A value of $\Delta R_{max} = 0.72$ was found for the PEG_{113}-*b*-$(TPE\text{-}TMC)_{20}$ monolayer at 5 nm^{-2}, i.e., 0.2 nm^2 per TPE group. Therefore a complete trilayer was formed in the case of the PEG_{113}-*b*-$(TPE\text{-}TMC)_n$ polymer series with no bilayer contribution as confirmed by the intensity value of UV-vis reflection spectroscopy.

Remarkably, the trilayer appeared as the limiting supramolecular structure formed at the air/liquid interface. Further reduction of the available surface area did not allow for additional multilayers, instead leading to solubilization of the excess PEG_{113}-*b*-$(TPE\text{-}TMC)_{20}$ molecules into the bulk water, as revealed by the constant value of ΔR_{max} upon further reduction of the available surface area, see Figure 2B. Similar values were found for the PEG_{113}-*b*-$(TPE\text{-}TMC)_n$ polymer series, indicating that in this case the increased length of the PEG_{113} block led in all cases to a complete trilayer structure, see S12-19. Therefore, the first kink observed for both isotherms of PEG_{113} and PEG_{45} polymers corresponds to the transition from monolayer to trilayer. A complete

trilayer is formed for the PEG_{113} polymers. On the other hand, the second kink obtained for the isotherms of the PEG_{45} polymers indicates a rearrangement and a loss of polymer molecules into the subphase leading to an incomplete trilayer.

The aggregation of the P(TPE-TMC) block could be monitored by following the position of the UV-vis reflection peak at ca. 320 nm as a function of the available surface area, see Figure 2C. The position of this peak in bulk solution showing no aggregation was λ_{max} = 316 nm. A slight difference with respect to the bulk solution was found with λ_{max} at ca. 317-320 nm for the PEG_{45}-*b*-$P(TPE\text{-}TMC)_8$ monolayer at high values of available surface area. The peak shifted to λ_{max} = 324 nm for a highly reduced surface area, indicating a significant aggregation of the TPE-TMC group. The PEG_{113}-*b*-$P(TPE\text{-}TMC)_{20}$ monolayer displayed the position of the UV-vis peak overlapping with that of the bulk solution. With a reduction of the available surface area from ca. 1 nm^2 to 0.45 nm^2 per P(TPE-TMC) block a shift to λ_{max} = 320 nm was found. Further reduction of the surface area to 0.15 nm^2 led to an increased shift to λ_{max} = 325 nm, indicating a high degree of aggregation.

The orientation factor could be calculated from the UV-vis reflection spectra using equation (2), displaying a value close to unity for the PEG_{45}-*b*-$P(TPE\text{-}TMC)_8$ and PEG_{113}-*b*-$P(TPE\text{-}TMC)_{20}$, see Figure 2D. A distribution of orientation of the P(TPE-TMC) block with respect to the air/liquid interface close to a random distribution was therefore obtained, in agreement with the aggregation and multilayered structures. A similar distribution was obtained for all amphiphilic copolymers, see S12-19.

Computer simulations offered detailed insights in the molecular nanostructure of the PEG_{45}-*b*-$P(TPE\text{-}TMC)_8$ polymer molecules.[43] A monolayer arrangement corresponding to high values of available surface area and a bilayer arrangement corresponding to lower values of surface area were considered, see Figure 3. The computer simulations were based on the Molecular Dynamics

methods, see Supporting Information for computational details. Significant differences were found between the two arrangements. The obtained area per $(PEG)_{45}$-*b*-$P(TPE\text{-}TMC)_8$ molecule was slightly reduced when comparing the monolayer to the bilayer, with values of area per molecule of 0.62 and 0.59 nm^2, respectively. This reduction in the available surface area pointed to an enhanced ordering when multilayered structures were formed.

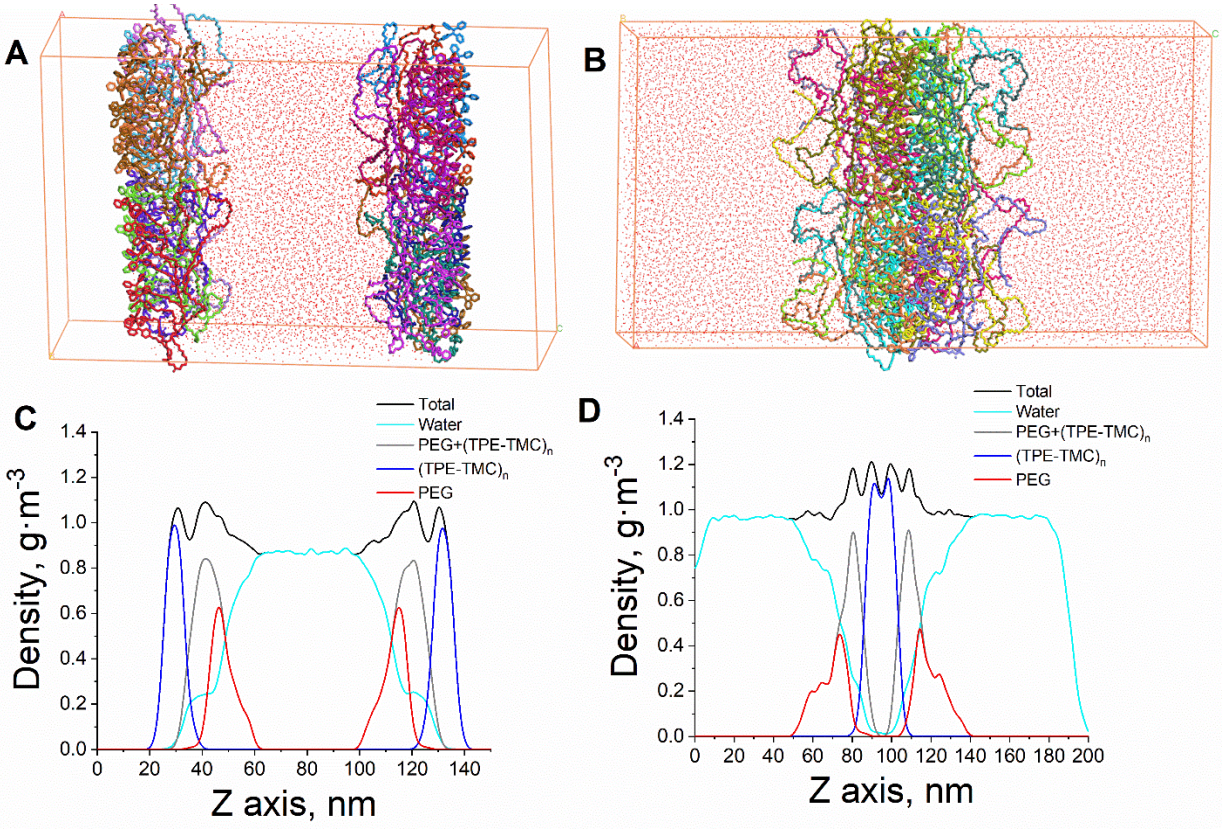

Figure 3. Molecular dynamics simulations unravel the molecular arrangement of the AIE polymers in mono- and multi-layer. Snapshot of the molecular dynamics simulation of the PEG_{45}-*b*-$P(TPE\text{-}TMC)_8$: A) monolayers and B) bilayers. Density of the P(TPE-TMC) block, PEG block and water in $g \cdot m^{-3}$ along the z-axis for the C) monolayer arrangement and D) bilayer arrangement.

H-bonding has been reported as the guiding interaction for self-assembly promoting AIE, leading to rigid assemblies as shown by Bravo et al.[44] A decrease in the number of the average number of H-bonds per PEG_{45}-*b*-$P(TPE\text{-}TMC)_8$ molecule with reduction in the surface area was observed, from 14.5 (monolayer) to 12.9 (bilayer). This partial loss of H-bonds pointed to a slight dehydration related with the enhanced intermolecular interactions between the PEG_{45}-*b*-$P(TPE\text{-}TMC)_8$ molecules. The number of H-bonds considering each monomer is comparatively lower to bulk conditions, as expected from the crowding of the AIE polymer molecules at the interface.[45,46] This increased interaction was additionally recorded as a decrease in the torsion angle formed by the C=C-C(phenyl)-C(phenyl) bonds, from 58.9º (monolayer) to 55.9º (bilayer), see Figure S20. Remarkably, the tilting angle of the mentioned torsion bond showed a lower variation when comparing monolayer to a bilayer, with values of 112.5º and 113.5º, respectively. Therefore, the restriction in the intramolecular movement by the increased crowding at the air/liquid interface leading to AIE did not significantly affect the supramolecular structure.

The photoluminescence (PL) spectra of the nanostructures formed by the amphiphilic polymers were obtained by transfer to a solid substrate.[47,48] There might be a modification of the ordering when transferring the polymer layers from the air/water interface to the solid substrate.[49] The 2D uniformity and roughness as well as other physical features might be assessed using Atomic Force Microscopy. Note that such study is beyond the scope of our present manuscript. The polymer layers were transferred by the Langmuir-Schaeffer technique at 0.4 nm^2 per monomer onto the silicon wafer prior to the vesicle formation. The absence of modification of the molecular arrangement of the P(TPE-TMC) groups when transferring the polymer layers was confirmed by the UV-vis spectra for the PEG_{113}-$P(TPE\text{-}TMC)_{32}$ polymer on the air/water interface and on glass solid substrates, see Figure S21. The PL spectra for the PEG_{45}-*b*-$P(TPE\text{-}TMC)_8$ and PEG_{113}-*b*-

P(TPE-TMC)$_{20}$ monolayers displayed AIE when the surface area reached ca. 0.4 nm^2 per monomer in opposition to the low PL of the monolayers transferred at 3.0 nm^2 per monomer, see Figure 4. The enhancement of the intensity of the fluorescence signal was ca. 25-fold for both cases. Note that the PL intensity was corrected by the available surface area per molecule of amphiphilic polymer, i.e., the enhancement of PL corresponds to AIE. The AIE was even visible by the naked eye under UV lamp illumination (λ_{exc} = 254 nm), see Figure 4C.

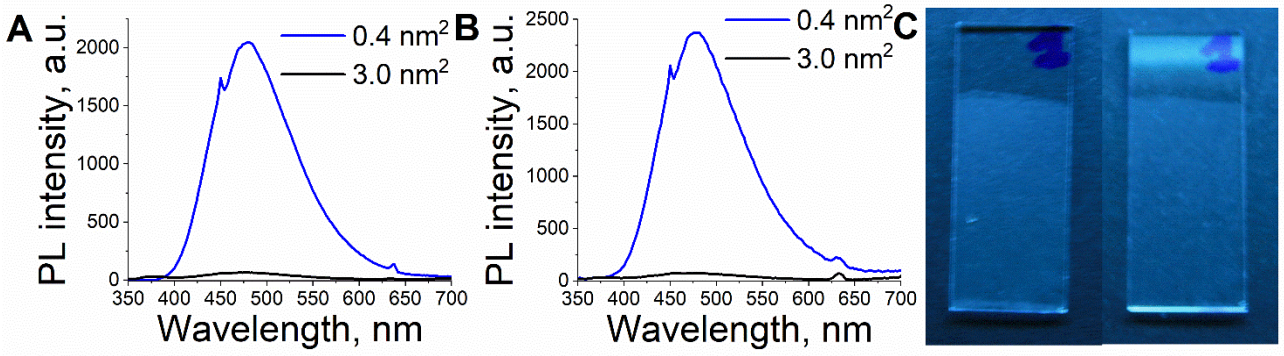

Figure 4. AIE from self-assembled nanostructures of the amphiphilic polymers. A) Photoluminescence (PL) spectra of PEG$_{45}$-*b*-P(TPE-TMC)$_8$ transferred to a quartz substrate. B) Photoluminescence (PL) spectra of PEG$_{113}$-*b*-P(TPE-TMC)$_{20}$ transferred to a quartz substrate. Blue line: available surface area of 0.4 nm^2 per polymer molecule. Black line: available surface area of 3.0 nm^2 per polymer molecule. Excitation wavelength: 315 nm. C) Photographs corresponding to the PEG$_{45}$-*b*-P(TPE-TMC)$_8$ and PEG$_{113}$-*b*-P(TPE-TMC)$_{20}$ layers (left and right, respectively) under lamp illumination with excitation wavelength: 254 nm. The photos were taken for polymer layers transferred at 0.4 nm^2 per monomer.

3D polymersomes could be readily obtained from the 2D trilayer by simply immersing the solid substrate in water with short application of ultrasound, see Figure 5. The application of ultrasound

have been shown to induce assembly onto AIE-gel structures.[50] The ultrasounds led to the detachment of the top bilayer in a similar manner to bubbling of supported lipid bilayers induced by chemical stimuli.[51] The two top layers of the amphiphilic polymer molecules were self-assembled onto polymersomes in water with a hydrodynamic diameter value of 122±51 nm as measured by Dynamic Light Scattering, see Figure 5. This procedure is easily applied to all amphiphilic polymer, as confirmed by the DLS measurements for polymersomes of PEG_{45}-*b*-$P(TPE\text{-}TMC)_8$ and PEG_{113}-*b*-$P(TPE\text{-}TMC)_{54}$, see S22. This value of hydrodynamic diameter was comparable to those found for similar f_{PEG}(wt%), as PEG_{45}-*b*-$P(TPE\text{-}TMC)_n$ polymersomes obtained by the nanoprecipitation method.[23] Lecommandoux et al. applied the nanoprecipitation method for the similar polymer PEG_{45}-*b*-$P(PTMC)_n$, but without TPE side chain in the polytrimethylcarbonate backbone, and obtained hydrodynamic diameter values around 100 nm for n = 170 and 332.[52] The fact that here $P(TPE\text{-}TMC)_n$ with comparatively shorter chains (n from 8 to 54) led to polymersomes with the similar hydrodynamic diameter values points at an enhanced interaction between the chains driven by the TPE group. Molecular weight of the hydrophobic blocks were comparable, with 19720 to 38512 Da for n = 170 and 332 for $P(PTMC)_n$ and 4728 to 31914 Da for n = 8 and 54 for $P(TPE\text{-}TMC)_n$. Note the π-π interaction could drive the assembly of polymer micelles.[53] The trilayer arrangement was further confirmed by contact angle measurements, see S23.

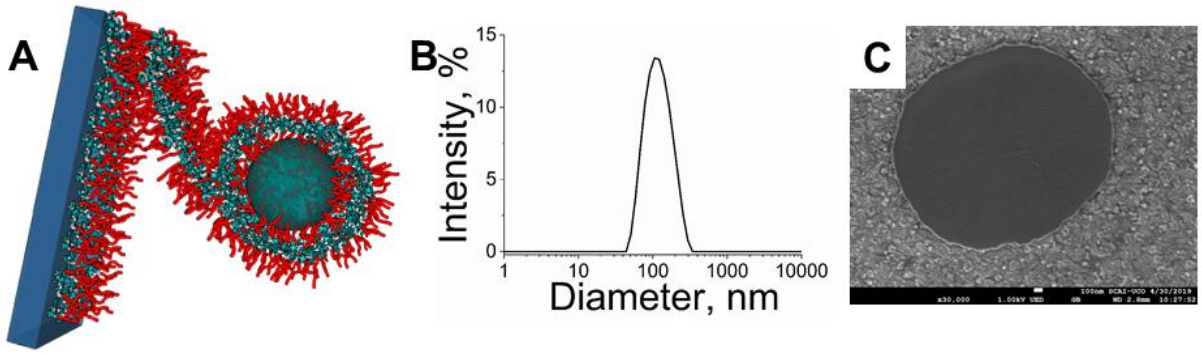

Figure 5. Formation of 3D AIE-polymersomes. A) Sketch of the formation process of polymersomes from deposited multilayers. B) Distribution of hydrodynamic diameter values of polymersomes formed from PEG_{113}-*b*-P(TPE-$TMC)_{32}$ obtained using Dynamic Light Scattering measurements. C) Scanning Electron Microscopy image of polymersomes from PEG_{113}-*b*-P(TPE-$TMC)_{32}$. Scale bar: 100 nm.

The dispersed polymersomes could also be observed using nanoparticle tracking analysis, see videos at Supporting Files. When observed by scanning electron microscopy, the polymersomes flocculated and flattened during the deposition and drying process to a final size of ca. 1.5 μm, see Figure 5C. This procedure for on-demand synthesis of polymersomes is an experimentally simple and fast protocol with no requirement of additional stimuli and separation techniques. Well-defined nanostructures at the air/liquid interface led to 3D polymersomes in colloidal dispersion. We anticipate that this process is a good candidate as a scalable and sustainable mass-production protocol for production of AIE-polymersomes.

CONCLUSIONS

Building on the previous knowledge on formation of AIE nanostructures [1,5,9,22], this study provides a molecularly detailed description on the assembly and arrangement of the AIE polymers at air/liquid interfaces. 2D nanostructures from a series of amphiphilic block copolymers PEG_m-*b*-P(TPE-TMC)$_n$ were achieved by using the Langmuir technique.[54] The study of the molecular arrangement included a combination of experiments and computer simulations. AIE fluorescence was achieved from the controlled aggregation of the TPE groups by adjusting the available surface area, similar to the described AIE by aggregation in 3D bulk conditions.[32] The AIE was successfully obtained by allocating a given available surface area to promote the controlled aggregation of the TPE-containing P(TPE-TMC) block. PEG_{113} polymers formed a complete trilayer at the air/liquid interface upon the maximum degree of compression, whereas PEG_{45} polymers formed multilayers with a distribution between bilayer and trilayer structure. The increase of the PEG length leads to a reduced area per polymer molecule at the air/liquid interface as noted by the Langmuir monolayer results. This trend is probably translated to the polymersomes and other nanostructures formed by amphiphilic copolymers using PEG as a hydrophilic block, as demonstrated for polymersomes obtained by nanoprecipitation.[23] 3D polymersomes were easily obtained from the 2D nanostructures by a simple application of ultrasounds. The insights include herein provide clues on the chemical design and balance between the hydrophilic and hydrophobic blocks when designing amphiphilic polymers for AIE self-assembled nanostructures. This work suggests that amphiphilic AIE-polymer at the air/liquid interface may provide highly tunable nanostructures for on-demand AIE properties.

ASSOCIATED CONTENT

Supporting Information. Experimental procedures, isotherms, Brewster Angle Microscopy pictures, UV-vis reflection spectra, molecular sketch, size distribution by dynamic light scattering

measurements and contact angle measurements. Videos of PEG_{113}-$P(TPE\text{-}TMC)_{32}$ observed by NanoTracking Analysis setup. The following files are available free of charge: Supporting_Information (PDF)

AUTHOR INFORMATION

Corresponding Author

*min-hui.li@chimieparistech.psl.eu (M.-H. L.), jjginer@uco.es (J. J. G.-C.)

Author Contributions

The manuscript was written through contributions of all authors. All authors have given approval to the final version of the manuscript. ‡These authors contributed equally.

ACKNOWLEDGMENT

Support from the Ministry of Science and Innovation of Spain through the MANA (CTQ2017-83961-R) and JEANS (CTQ2017-92264-EXP) projects is acknowledged. J.J.G.-C. acknowledges the Ministry of Science, Innovation and Universities for a "Ramon y Cajal" contract (RyC-2014-14956). Support from the Consejería de Economía, Innovación, Ciencia y Empleo (Junta de Andalucía) through the project UCO-1265871 (FEDER Andalucía 2014-2020) is acknowledged. Dr. Madueno from University of Córdoba is acknowledged for the assistance with the contact angle measurements. Francisco Gracia-Alfonso (SCAI, Universidad de Córdoba) is acknowledged for invaluable help with the electron microscopy. This work was also financially supported by the French National Research Agency (ANR-16-CE29-0028). Nian Zhang gratefully acknowledges the China Scholarship Council for funding her PhD scholarship.

REFERENCES

[1] W. Tuo, Y. Sun, S. Lu, X. Li, Y. Sun, P.J. Stang, Pillar[5]arene-Containing Metallacycles and Host–Guest Interaction Caused Aggregation-Induced Emission Enhancement Platforms, J. Am. Chem. Soc. 142 (2020) 16930–16934. doi:10.1021/jacs.0c08697.

[2] H.-T. Feng, Y. Li, X. Duan, X. Wang, C. Qi, J.W.Y. Lam, D. Ding, B.Z. Tang, Substitution Activated Precise Phototheranostics through Supramolecular Assembly of AIEgen and Calixarene, J. Am. Chem. Soc. 142 (2020) 15966–15974. doi:10.1021/jacs.0c06872.

[3] J. Mei, N.L.C. Leung, R.T.K. Kwok, J.W.Y. Lam, B.Z. Tang, Aggregation-Induced Emission: Together We Shine, United We Soar!, Chem. Rev. 115 (2015) 11718–11940. doi:10.1021/acs.chemrev.5b00263.

[4] Y. Tu, J. Liu, H. Zhang, Q. Peng, J.W.Y. Lam, B.Z. Tang, Restriction of Access to the Dark State: A New Mechanistic Model for Heteroatom-Containing AIE Systems, Angew. Chem. Int. Ed. 58 (2019) 14911–14914. doi:10.1002/anie.201907522.

[5] S. Xu, Y. Duan, B. Liu, Precise Molecular Design for High-Performance Luminogens with Aggregation-Induced Emission, Adv. Mater. 32 (2020) 1903530. doi:10.1002/adma.201903530.

[6] S. Feng, S. Gong, G. Feng, Aggregation-induced emission and solid fluorescence of fluorescein derivatives, Chem. Commun. 56 (2020) 2511–2513. doi:10.1039/C9CC09784H.

[7] Z. He, R. Jiang, W. Long, H. Huang, M. Liu, Y. Feng, N. Zhou, H. Ouyang, X. Zhang, Y. Wei, Red aggregation-induced emission luminogen and Gd^{3+} codoped mesoporous silica nanoparticles as dual-mode probes for fluorescent and magnetic resonance imaging, J. Colloid Interface Sci. 567 (2020) 136–144. doi:10.1016/j.jcis.2020.02.009.

[8] T. Zhang, Y. Li, Z. Zheng, R. Ye, Y. Zhang, R.T.K. Kwok, J.W.Y. Lam, B.Z. Tang, In Situ Monitoring Apoptosis Process by a Self-Reporting Photosensitizer, J. Am. Chem. Soc. 141 (2019) 5612–5616. doi:10.1021/jacs.9b00636.

[9] T. Xue, K. Shao, J. Xiang, X. Pan, Z. Zhu, Y. He, In situ construction of a self-assembled AIE probe for tumor hypoxia imaging, Nanoscale. 12 (2020) 7509–7513. doi:10.1039/D0NR00444H.

[10] W. Wu, Y. Yang, Y. Yang, Y. Yang, K. Zhang, L. Guo, H. Ge, X. Chen, J. Liu, H. Feng, Molecular Engineering of an Organic NIR-II Fluorophore with Aggregation-Induced Emission Characteristics for In Vivo Imaging, Small. 15 (2019) 1805549. doi:10.1002/smll.201805549.

[11] X. He, F. Yin, D. Wang, L.-H. Xiong, R.T.K. Kwok, P.F. Gao, Z. Zhao, J.W.Y. Lam, K.-T. Yong, Z. Li, B.Z. Tang, AIE Featured Inorganic–Organic Core@Shell Nanoparticles for High-Efficiency siRNA Delivery and Real-Time Monitoring, Nano Lett. 19 (2019) 2272–2279. doi:10.1021/acs.nanolett.8b04677.

[12] X. Cai, D. Mao, C. Wang, D. Kong, X. Cheng, B. Liu, Multifunctional Liposome: A Bright AIEgen-Lipid Conjugate with Strong Photosensitization, Angew. Chem. Int. Ed. 57 (2018) 16396–16400. doi:10.1002/anie.201809641.

[13] M. Kang, C. Zhou, S. Wu, B. Yu, Z. Zhang, N. Song, M.M.S. Lee, W. Xu, F.-J. Xu, D. Wang, L. Wang, B.Z. Tang, Evaluation of Structure–Function Relationships of Aggregation-Induced Emission Luminogens for Simultaneous Dual Applications of Specific Discrimination and Efficient Photodynamic Killing of Gram-Positive Bacteria, J. Am. Chem. Soc. 141 (2019) 16781–16789. doi:10.1021/jacs.9b07162.

[14] C. Zhou, M. Jiang, J. Du, H. Bai, G. Shan, R.T.K. Kwok, J.H.C. Chau, J. Zhang, J.W.Y.

Lam, P. Huang, B.Z. Tang, One stone, three birds: one AIEgen with three colors for fast differentiation of three pathogens, Chem. Sci. 11 (2020) 4730–4740. doi:10.1039/D0SC00256A.

[15] C. Yang, F. Hu, X. Zhang, C. Ren, F. Huang, J. Liu, Y. Zhang, L. Yang, Y. Gao, B. Liu, J. Liu, Combating bacterial infection by in situ self-assembly of AIEgen-peptide conjugate, Biomaterials. 244 (2020) 119972. doi:10.1016/j.biomaterials.2020.119972.

[16] X. Chen, H. Gao, Y. Deng, Q. Jin, J. Ji, D. Ding, Supramolecular Aggregation-Induced Emission Nanodots with Programmed Tumor Microenvironment Responsiveness for Image-Guided Orthotopic Pancreatic Cancer Therapy, ACS Nano. 14 (2020) 5121–5134. doi:10.1021/acsnano.0c02197.

[17] Z. Qiu, W. Zhao, M. Cao, Y. Wang, J.W.Y. Lam, Z. Zhang, X. Chen, B.Z. Tang, Dynamic Visualization of Stress/Strain Distribution and Fatigue Crack Propagation by an Organic Mechanoresponsive AIE Luminogen, Adv. Mater. 30 (2018) 1803924. doi:10.1002/adma.201803924.

[18] D. Zhang, Y. Fan, H. Chen, S. Trépout, M.-H. Li, CO2-activated reversible transition between polymersomes and micelles with AIE fluorescence, Angew. Chem. Int. Ed. (2019). doi:10.1002/anie.201905089.

[19] Y.-L. Wang, C. Li, H.-Q. Qu, C. Fan, P.-J. Zhao, R. Tian, M.-Q. Zhu, Real-Time Fluorescence In Situ Visualization of Latent Fingerprints Exceeding Level 3 Details Based on Aggregation-Induced Emission, J. Am. Chem. Soc. 142 (2020) 7497–7505. doi:10.1021/jacs.0c00124.

[20] J.M. Delente, D. Umadevi, S. Shanmugaraju, O. Kotova, G.W. Watson, T. Gunnlaugsson, Aggregation induced emission (AIE) active 4-amino-1,8-naphthalimide-Tröger's base for

the selective sensing of chemical explosives in competitive aqueous media, Chem. Commun. 56 (2020) 2562–2565. doi:10.1039/C9CC08457F.

[21] M. Collot, J. Schild, K.T. Fam, R. Bouchaala, A.S. Klymchenko, Stealth and Bright Monomolecular Fluorescent Organic Nanoparticles Based on Folded Amphiphilic Polymer, ACS Nano. 14 (2020) 13924–13937. doi:10.1021/acsnano.0c06348.

[22] Y. Niu, B. Zhang, M. Galluzzi, An amphiphilic aggregate-induced emission polyurethane probe for in situ actin observation in living cells, J. Colloid Interface Sci. 582 (2021) 1191–1202. doi:10.1016/j.jcis.2020.08.113.

[23] N. Zhang, H. Chen, Y. Fan, L. Zhou, S. Trépout, J. Guo, M.-H. Li, Fluorescent Polymersomes with Aggregation-Induced Emission, ACS Nano. 12 (2018) 4025–4035. doi:10.1021/acsnano.8b01755.

[24] A.P. Dias, S. da Silva Santos, J.V. da Silva, R. Parise-Filho, E. Igne Ferreira, O. El Seoud, J. Giarolla, Dendrimers in the context of nanomedicine, Int. J. Pharm. 573 (2020) 118814. doi:10.1016/j.ijpharm.2019.118814.

[25] T.-T. Wang, Q.-C. Wei, Z.-T. Zhang, M.-T. Lin, J.-J. Chen, Y. Zhou, N.-N. Guo, X.-C. Zhong, W.-H. Xu, Z.-X. Liu, M. Han, J.-Q. Gao, AIE/FRET-based versatile PEG-Pep-TPE/DOX nanoparticles for cancer therapy and real-time drug release monitoring, Biomater. Sci. 8 (2020) 118–124. doi:10.1039/C9BM01546A.

[26] Y.-H. Zhang, X. Li, L. Huang, H.S. Kim, J. An, M. Lan, Q.-Y. Cao, J.S. Kim, AIE based GSH activatable photosensitizer for imaging-guided photodynamic therapy, Chem. Commun. 56 (2020) 10317–10320. doi:10.1039/D0CC02045A.

[27] A. Rananaware, R.S. Bhosale, H. Patil, M. Al Kobaisi, A. Abraham, R. Shukla, S. V. Bhosale, S. V. Bhosale, Precise aggregation-induced emission enhancement via H^+ sensing

and its use in ratiometric detection of intracellular pH values, RSC Adv. 4 (2014) 59078–59082. doi:10.1039/C4RA10511G.

[28] Y. Chen, Z. Huang, X. Liu, L. Mao, J. Yuan, X. Zhang, L. Tao, Y. Wei, A novel AIE-active dye for fluorescent nanoparticles by one-pot combination of Hantzsch reaction and RAFT polymerization: synthesis, molecular structure and application in cell imaging, RSC Adv. 9 (2019) 32601–32607. doi:10.1039/C9RA06452D.

[29] C. Rubia-Payá, G. De Miguel, M.T. Martín-Romero, J.J. Giner-Casares, L. Camacho, UV-Vis Reflection-Absorption Spectroscopy at air-liquid interfaces, Adv. Colloid Interface Sci. 225 (2015) 134–145. doi:10.1016/j.cis.2015.08.012.

[30] J.P. Coelho, M.J. Mayoral, L. Camacho, M.T. Martín-Romero, G. Tardajos, I. López-Montero, E. Sanz, D. Ávila-Brande, J.J. Giner-Casares, G. Fernández, A. Guerrero-Martínez, Mechanosensitive gold colloidal membranes mediated by supramolecular interfacial self-assembly, J. Am. Chem. Soc. 139 (2017) 1120–1128. doi:10.102l/Jacs.6b09485.

[31] S. Kim, M. Ju, J. Lee, J. Hwang, J. Lee, Polymer Interfacial Self-Assembly Guided Two-Dimensional Engineering of Hierarchically Porous Carbon Nanosheets, J. Am. Chem. Soc. 142 (2020) 9250–9257. doi:10.1021/jacs.0c00311.

[32] H. Liu, Y. Gu, Y. Dai, K. Wang, S. Zhang, G. Chen, B. Zou, B. Yang, Pressure-Induced Blue-Shifted and Enhanced Emission: A Cooperative Effect between Aggregation-Induced Emission and Energy-Transfer Suppression, J. Am. Chem. Soc. 142 (2020) 1153–1158. doi:10.1021/jacs.9b11080.

[33] C.A. Naumann, C.F. Brooks, G.G. Fuller, W. Knoll, C.W. Frank, Viscoelastic Properties of Lipopolymers at the Air−Water Interface: A Combined Interfacial Stress Rheometer and

Film Balance Study, Langmuir. 15 (1999) 7752–7761. doi:10.1021/la990261q.

[34] R.L.C.G. da Silva, S.K. Sharma, S. Paudyal, K.J. Mintz, L. Caseli, R.M. Leblanc, Surface chemistry and spectroscopic studies of the native phenylalanine dehydrogenase Langmuir monolayer at the air/aqueous NaCl interface, J. Colloid Interface Sci. 560 (2020) 458–466. doi:10.1016/j.jcis.2019.10.086.

[35] F.A. de S. Furtado, J.F.B. Escobar, A.M. Martinez, C. Giordani, J.M.A. Caiut, L. Caseli, C. Molina, Molecular Information on the Potential of Europium Complexes for Local Recognition of a Nucleoside-Based Drug by Using Nanostructured Interfaces Assembled as Langmuir–Blodgett Films, Langmuir. 36 (2020) 3843–3852. doi:10.1021/acs.langmuir.0c00708.

[36] D. Liu, M. Chen, K. Li, Z. Li, J. Huang, J. Wang, Z. Jiang, Z. Zhang, T. Xie, G.R. Newkome, P. Wang, Giant Truncated Metallo-Tetrahedron with Unexpected Supramolecular Aggregation Induced Emission Enhancement, J. Am. Chem. Soc. 142 (2020) 7987–7994. doi:10.1021/jacs.0c02366.

[37] Y. Zhao, X. Zhao, M. Li, Z. Li, H. Peng, X. Xie, Crosstalk-Free Patterning of Cooperative-Thermoresponse Images by the Synergy of the AIEgen with the Liquid Crystal, Angew. Chem. Int. Ed. 59 (2020) 10066–10072. doi:10.1002/anie.201915053.

[38] H.-Q. Peng, B. Liu, P. Wei, P. Zhang, H. Zhang, J. Zhang, K. Li, Y. Li, Y. Cheng, J.W.Y. Lam, W. Zhang, C.-S. Lee, B.Z. Tang, Visualizing the Initial Step of Self-Assembly and the Phase Transition by Stereogenic Amphiphiles with Aggregation-Induced Emission, ACS Nano. 13 (2019) 839–846. doi:10.1021/acsnano.8b08358.

[39] N. Jiang, D. Zhu, Z. Su, M.R. Bryce, Blue-emitting thermoreversible oligourethane gelators with aggregation-induced emission properties, J. Mater. Chem. C. 8 (2020) 5137–5142.

doi:10.1039/D0TC00757A.

[40] A.M. Gonçalves Da Silva, E.J.M. Filipe, J.M.R. D'Oliveira, J.M.G. Martinho, Interfacial behavior of poly(styrene)-poly(ethylene oxide) diblock copolymer monolayers at the air-water interface. Hydrophilic block chain length and temperature influence, Langmuir. 12 (1996) 6547–6553.

[41] V. Tsukanova, C. Salesse, High-Pressure Transition of a Poly(ethylene glycol)-Grafted Phospholipid Monolayer at the Air/Water Interface, Macromolecules. 36 (2003) 7227–7235. doi:10.1021/ma0257806.

[42] E. Jiménez-Millan, J.J. Giner-Casares, M.T.M.T. Martín-Romero, G. Brezesinski, L. Camacho, Chiral textures inside 2D achiral domains, J. Am. Chem. Soc. 133 (2011) 19028–19031. doi:10.1021/ja206037k.

[43] F. Jiménez-Ángeles, H.-K. Kwon, K. Sadman, T. Wu, K.R. Shull, M. Olvera de la Cruz, Self-Assembly of Charge-Containing Copolymers at the Liquid–Liquid Interface, ACS Cent. Sci. 5 (2019) 688–699. doi:10.1021/acscentsci.9b00084.

[44] P.J. Pacheco-Liñán, C. Martín, C. Alonso-Moreno, A. Juan, D. Hermida-Merino, A. Garzón-Ruíz, J. Albaladejo, M. Van der Auweraer, B. Cohen, I. Bravo, The role of water and influence of hydrogen bonding on the self-assembly aggregation induced emission of an anthracene-guanidine-derivative, Chem. Commun. 56 (2020) 4102–4105. doi:10.1039/D0CC00990C.

[45] E.M. Adams, C.B. Casper, H.C. Allen, Effect of cation enrichment on dipalmitoylphosphatidylcholine (DPPC) monolayers at the air-water interface, J. Colloid Interface Sci. 478 (2016) 353–364. doi:10.1016/j.jcis.2016.06.016.

[46] E.M. Adams, B.A. Wellen, R. Thiraux, S.K. Reddy, A.S. Vidalis, F. Paesani, H.C. Allen,

Sodium–carboxylate contact ion pair formation induces stabilization of palmitic acid monolayers at high pH, Phys. Chem. Chem. Phys. 19 (2017) 10481–10490. doi:10.1039/C7CP00167C.

[47] T.A.F. König, P.A. Ledin, J. Kerszulis, M.A. Mahmoud, M.A. El-Sayed, J.R. Reynolds, V. V. Tsukruk, Electrically Tunable Plasmonic Behavior of Nanocube–Polymer Nanomaterials Induced by a Redox-Active Electrochromic Polymer, ACS Nano. 8 (2014) 6182–6192. doi:10.1021/nn501601e.

[48] J.-W. Liu, J.-H. Zhu, C.-L. Zhang, H.-W. Liang, S.-H. Yu, Mesostructured Assemblies of Ultrathin Superlong Tellurium Nanowires and Their Photoconductivity, J. Am. Chem. Soc. 132 (2010) 8945–8952. doi:10.1021/ja910871s.

[49] H. Moehwald, G. Brezesinski, From Langmuir Monolayers to Multilayer Films, Langmuir. 32 (2016) 10445–10458. doi:10.1021/acs.langmuir.6b02518.

[50] J. Guo, X. Yu, Z. Zhang, Y. Li, Self-healing gels triggered by ultrasound with color-tunable emission based on ion recognition, J. Colloid Interface Sci. 540 (2019) 134–141. doi:10.1016/j.jcis.2019.01.012.

[51] M.F. Poyton, S. Pullanchery, S. Sun, T. Yang, P.S. Cremer, Zn^{2+} Binds to Phosphatidylserine and Induces Membrane Blebbing, J. Am. Chem. Soc. 142 (2020) 18679–18686. doi:10.1021/jacs.0c09103.

[52] C. Lebleu, L. Rodrigues, J.-M. Guigner, A. Brûlet, E. Garanger, S. Lecommandoux, Self-Assembly of PEG-*b*-PTMC Copolymers: Micelles and Polymersomes Size Control, Langmuir. 35 (2019) 13364–13374. doi:10.1021/acs.langmuir.9b02264.

[53] C. Liang, X. Bai, C. Qi, Q. Sun, X. Han, T. Lan, H. Zhang, X. Zheng, R. Liang, J. Jiao, Z. Zheng, J. Fang, P. Lei, Y. Wang, D. Möckel, J.M. Metselaar, G. Storm, W.E. Hennink, F.

Kiessling, H. Wei, T. Lammers, Y. Shi, B. Wei, Π electron-stabilized polymeric micelles potentiate docetaxel therapy in advanced-stage gastrointestinal cancer, Biomaterials. 266 (2021) 120432. doi:10.1016/j.biomaterials.2020.120432.

[54] J.J. Giner-Casares, G. Brezesinski, H. Möhwald, Langmuir monolayers as unique physical models, Curr. Opin. Colloid Interface Sci. 19 (2014) 176–182. doi:10.1016/j.cocis.2013.07.006.

GRAPHICAL ABSTRACT

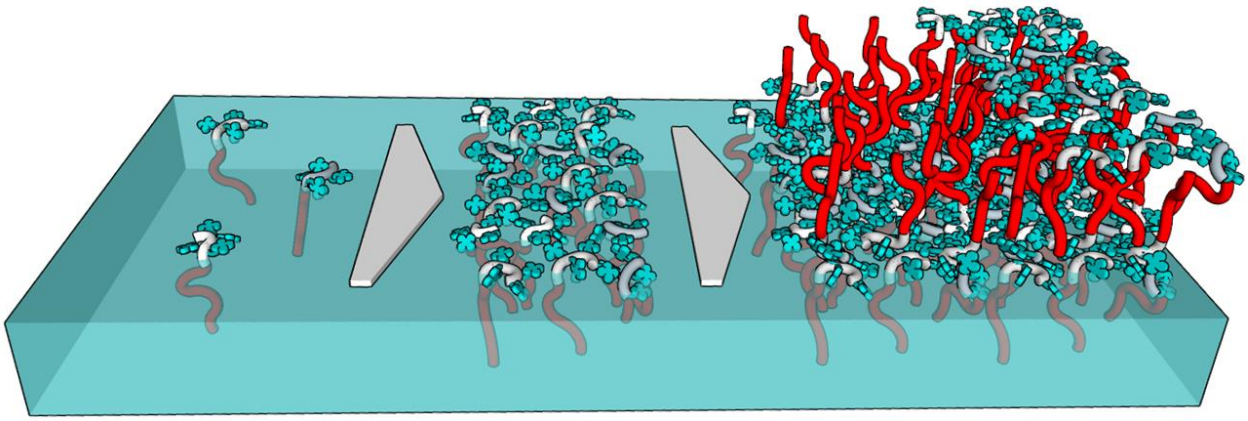

FIGURE CAPTIONS

Figure 1. 2D self-assembly and in situ UV-vis reflection spectroscopy of AIE polymers. A) Molecular structure of the PEG_m-*b*-$P(TPE\text{-}TMC)_n$ polymer. B) Sketch depicting the self-assembly of the PEG_m-*b*-$P(TPE\text{-}TMC)_n$ polymer at the air/water interface C) Surface pressure – molecular area isotherms for the PEG_{45} polymer derivatives. D) Surface pressure – molecular area isotherms for the PEG_{113} polymer derivatives. E) UV-vis reflection spectra of the PEG_{45}-*b*-$P(TPE\text{-}TMC)_8$ monolayer recorded from 3.7 to 0.2 nm^2 per TPE monomer.

Figure 2. In situ UV-vis reflection spectroscopy for the AIE-polymers at the air/liquid interface. Top: PEG_{45}-*b*-$(TPE\text{-}TMC)_8$ monolayer. Bottom: PEG_{113}-*b*-$(TPE\text{-}TMC)_{20}$ monolayer. A) Left: difference normalized UV-vis reflection spectra. Right: Bulk UV-vis spectrum (black line). Inset: values of area per P(TPE-TMC) block. B) Maximum value of intensity of UV-vis reflection. C) Left, position of the UV-vis reflection peak (black circles). Dashed line corresponds to the peak position for the UV-vis absorbance spectrum in bulk solution. Right, orientation factor for the TPE groups (blue triangles).

Figure 3. Molecular dynamics simulations unravel the molecular arrangement of the AIE polymers in mono- and multi-layer. Snapshot of the molecular dynamics simulation of the PEG_{45}-*b*-$P(TPE\text{-}TMC)_8$: A) monolayers and B) bilayers. Density of the P(TPE-TMC) block, PEG block and water in $g \cdot m^{-3}$ along the z-axis for the C) monolayer arrangement and D) bilayer arrangement.

Figure 4. AIE from self-assembled nanostructures of the amphiphilic polymers. A) Photoluminescence (PL) spectra of PEG_{45}-*b*-$P(TPE\text{-}TMC)_8$ transferred to a quartz substrate. B) Photoluminescence (PL) spectra of PEG_{113}-*b*-$P(TPE\text{-}TMC)_{20}$ transferred to a quartz substrate.

Blue line: available surface area of 0.4 nm^2 per polymer molecule. Black line: available surface area of 3.0 nm^2 per polymer molecule. Excitation wavelength: 315 nm. C) Photographs corresponding to the PEG_{45}-*b*-$P(TPE\text{-}TMC)_8$ and PEG_{113}-*b*-$P(TPE\text{-}TMC)_{20}$ layers (left and right, respectively) under lamp illumination with excitation wavelength: 254 nm. The photos were taken for polymer layers transferred at 0.4 nm^2 per monomer.

Figure 5. Formation of 3D AIE-polymersomes. A) Sketch of the formation process of polymersomes from deposited multilayers. B) Distribution of hydrodynamic diameter values of polymersomes formed from PEG_{113}-*b*-$P(TPE\text{-}TMC)_{32}$ obtained using Dynamic Light Scattering measurements. C) Scanning Electron Microscopy image of polymersomes from PEG_{113}-*b*-$P(TPE\text{-}TMC)_{32}$. Scale bar: 100 nm.

TABLES

Table 1. Chemical composition of the $(PEG)_m$-*b*-$P(TPE\text{-}TMC)_n$ derivatives.

PEG_{45}-*b*-$P(TPE\text{-}TMC)_n$			
Polymer name	Mn[a]	PDI[b]	f_{PEG} (%)[a]
PEG_{45}-*b*-$P(TPE\text{-}TMC)_8$	6800	1.34	29
PEG_{45}-*b*-$P(TPE\text{-}TMC)_{10}$	8100	-	25
PEG_{45}-*b*-$P(TPE\text{-}TMC)_{13}$	9600	1.35	21
PEG_{45}-*b*-$P(TPE\text{-}TMC)_{26}$	17100	-	12
PEG_{45}-*b*-$P(TPE\text{-}TMC)_{32}$	20900	1.44	9.6
PEG_{113}-*b*-$P(TPE\text{-}TMC)_n$			
Polymer name	Mn[a]	PDI[b]	f_{PEG} (%)[a]
PEG_{113}-*b*-$P(TPE\text{-}TMC)_{13}$	12700	1.47	39
PEG_{113}-*b*-$P(TPE\text{-}TMC)_{20}$	17100	1.36	29
PEG_{113}-*b*-$P(TPE\text{-}TMC)_{32}$	23900	1.37	21
PEG_{113}-*b*-$P(TPE\text{-}TMC)_{45}$	31400	1.47	16
PEG_{113}-*b*-$P(TPE\text{-}TMC)_{54}$	37000	1.44	13.5

[a]The number-average molecular weight (M_n) and the hydrophilic weight ratio (over the total copolymer) (f_{PEG}) of the copolymer were determined by ^1H NMR spectroscopy.

[b]PDI = Mw/Mn; Mw and Mn here were measured by size exclusion chromatography using THF as eluent and monodispersed polystyrenes as calibration standards.